J. Fluid Mech. (2011), *vol.* 689, *pp.* 357–375. © Cambridge University Press 2011
doi:10.1017/jfm.2011.420

Solid–mush interface conditions for mushy layers

Nicholas R. Gewecke[1]† **and Tim P. Schulze**[2]

[1] Department of Mathematical Sciences, University of Delaware, Newark, DE 19716, USA
[2] Department of Mathematics, University of Tennessee, Knoxville, TN 37996-0614, USA

(Received 1 July 2011; revised 1 July 2011; accepted 22 September 2011;
first published online 16 November 2011)

A subtle issue in the study of mushy zones which form during the solidification of binary alloys is that there are two distinct types of solid–mush interfaces which may occur. One of these is a eutectic front and the other is a front which separates the mushy layer and, assuming complete solute rejection, a layer of pure solid. For semi-infinite-domain configurations that admit similarity solutions, such as those at a uniform initial temperature and concentration with an imposed cold temperature at the lower boundary, only one of the two types appears, and the type of front is determined by the various parameters of the system. In a finite domain, it is possible for each type of front to appear at different times. Specifically, the advance of the eutectic front is restricted by the isotherm associated with the eutectic temperature, and the other front type will appear over a longer time scale. Leading up to the time when the front changes type, the concentration being frozen into the solid decreases. This process writes a history of the system into the solid.

Key words: solidification/melting

1. Introduction

Solidification of a binary alloy from a cold boundary can result in a variety of phenomena. First, a planar solid–liquid front can advance from the cold boundary. Second, if the temperature at the lower boundary is in an appropriate range, a mushy zone can appear as the result of an instability caused by a build-up of solute ahead of the solidification front. We are concerned with the behaviour of the system when a mushy layer is present.

A typical experimental arrangement consists of a tank filled with a uniform solution at a uniform temperature placed upon a cold surface. If the system is arranged in such a way that a mushy zone will appear, two different sets of conditions at the solid–mush interface are possible, and the temperature field plays an important role in determining which set applies. The two sets of conditions at the solid–mush interface can be described as a diffusion-controlled front and a $T = T_E$ front, where T_E denotes the eutectic temperature, at which solidification occurs regardless of the concentration of the alloy. Both of these possibilities were permitted in models studied by

† Email address for correspondence: ngewecke@math.udel.edu

https://doi.org/10.1017/jfm.2011.420 Published online by Cambridge University Press

Fowler (1985) and Emms & Fowler (1994). These studies are primarily concerned with the occurrence of convective instabilities, with Fowler (1985) using a basic state solution containing prescribed motion of the solid–mush and mush–liquid interfaces.

On the other hand, we are more interested in the solutions of the free-boundary problems, which have been addressed in the context of similarity solutions by Worster (1986) and Anderson (2003). The results of Anderson (2003) are for ternary alloys, but can be modified to apply to binary alloys. Worster (1986) considered the case where the temperature at the bottom of the tank is no colder than the eutectic, so the solid–mush interface is controlled by solute diffusion. On the other hand, Anderson (2003) considers the case where the bottom of the tank is very cold, so that a $T = T_E$ front describes the solid–mush interface. In other words, it is clear that the results of Worster (1986) apply when $T_B \geqslant T_E$ and the results of Anderson (2003) apply when T_B is sufficiently below T_E. For values of T_B below but still near T_E, the eutectic isotherm can appear below the diffusion-controlled front. This indicates that there is some critical temperature at the base T_B^* where the front type changes. Both of these prior studies utilize similarity solutions, and each of the fronts for these similarity solutions can be written in the form

$$h(t) = \alpha\sqrt{\kappa t}. \tag{1.1}$$

Only one of the two possibilities occurs for a given set of parameters. Determining which of the front types is present can be done by calculating the similarity solution given by Worster (1986) and then checking the interface temperature, but we will discuss a method for identifying the critical temperature T_B^* at the base of the tank, with other parameters fixed, at which the switch between the two interface conditions occurs.

In a finite tank, the issue becomes more complicated. The upper and lower boundaries are held at fixed temperatures, so the $T = T_E$ isotherm reaches a finite depth steady state that can be easily determined. However, once the $T = T_E$ isotherm slows sufficiently, solute diffusion can begin to drive the advance of the solid–mush interface. In other words, both cases can occur as the solidification progresses.

This is different from what occurs in the absence of solute diffusion. In such a case, the solid–mush interface follows the $T = T_E$ isotherm exactly if the lower boundary is cooled below $T = T_E$, or never appears if that cold boundary is fixed above the eutectic temperature. This is essentially the behaviour described by Emms & Fowler (1994), where latent heat was included with the velocity of the solid–mush interface given by either the Stefan condition, if eutectic, or being approximately zero otherwise. However, as demonstrated in Worster (1986) and Gewecke & Schulze (2011), solute diffusion can still drive the advance of a solid–mush interface even when the temperature at the bottom of the tank is above the eutectic. This effect also appears more generally when the solid–mush interface is not eutectic, even if the base of the tank is fixed at a sub-eutectic temperature. Hence, the two possibilities for the interface are eutectic, when $T = T_E$ at the interface, or diffusion-controlled.

The behaviour in a finite tank without the possibility of a $T = T_E$ front has already been studied by Gewecke & Schulze (2011). In that study, the temperature at the base of the tank is restricted so that $T_B > T_E$. An assumption of negligible latent heat permitted the application of the method of characteristics to the problem. We will take a similar approach to the more general case, where we require only that T_B is cold enough to cause formation of a mushy layer. The previous study demonstrated that the mushy layer will eventually vanish. This is due to the mush–liquid interface being restricted by a particular isotherm and the advance of the solid–mush interface being

https://doi.org/10.1017/jfm.2011.420 Published online by Cambridge University Press

driven by solute diffusion, and these two eventually intersect. In the present case, the mushy layer will still vanish on a finite domain.

A major focus of this paper is to identify when certain conditions apply at the solid–mush interface. In contrast, conditions at mush–liquid interfaces have previously been studied by Worster (1986) for growth from a cold boundary in an infinite domain, by Schulze & Worster (1999, 2005) for the case of crystal pulling, and by Gewecke & Schulze (2011) for growth from a cold boundary on a finite domain. The conditions to apply in each case depend upon the interface velocity, and often involve some other velocity arising in the system. We follow an approach similar to that used by Gewecke & Schulze (2011), where the interface velocity can be compared with the velocity of a characteristic at the interface to identify the applicable conditions at a given time. In the present case, we will find that the interface follows the eutectic isotherm until the velocity of that isotherm falls below the velocity of a characteristic at the interface.

The assumption of negligible latent heat is used to simplify the mathematical analysis of the problem. The primary benefit of this assumption is that the temperature field no longer depends upon other quantities in the problem. While the presence of latent heat would serve to slow the solidification in the system, the transition from a eutectic solid–mush interface to a diffusion-controlled solid–mush interface would still appear. Negligible latent heat has also been used in other studies of binary alloy solidification, especially in studies of directional solidification of alloys such as Langer (1980) and the results reviewed by Davis (2001).

We will first review the model for an infinite domain and discuss our simplifying assumptions. Then, we will investigate the issues for the infinite domain that we have discussed above, identifying a method to determine which of the two conditions determines the location of the solid–mush interface. After that, we will describe the changes for the model associated with a finite domain. We will then identify our method for numerically solving the finite-domain model. Results will be presented and discussed, illustrating the transition discussed above.

2. Infinite-domain case

The two cases we are concerned with differ only at the solid–mush interface. We will present the model as given by Worster (1986) with complete solute rejection and a non-eutectic solid–mush front, and then describe the modified interface conditions due to a eutectic front. For both cases, we assume equal thermal properties in all phases and total solute rejection from a non-eutectic solid. Here, we present the model with latent heat, but we will later assume that latent heat is negligible. Let $a(t)$ denote the solid–mush front and $b(t)$ denote the mush–liquid front.

In the far field, $z \to \infty$,

$$T \to T_\infty, \tag{2.1a}$$

$$C \to C_0, \tag{2.1b}$$

where T denotes temperature and C denotes the concentration of solute in the liquid phase.

In the liquid region, $b(t) < z$,

$$\frac{\partial T}{\partial t} = \kappa \frac{\partial^2 T}{\partial z^2}, \tag{2.2a}$$

$$\frac{\partial C}{\partial t} = D \frac{\partial^2 C}{\partial z^2}, \tag{2.2b}$$

where κ and D are the thermal and solutal diffusivities, respectively.

https://doi.org/10.1017/jfm.2011.420 Published online by Cambridge University Press

At the mush–liquid interface, $z = b(t)$,

$$[T]_{-}^{+} = 0, \tag{2.3a}$$

$$[C]_{-}^{+} = 0, \tag{2.3b}$$

$$\frac{L}{c_p}(1-\chi_b)\,\dot{b} = \kappa\left(\frac{\partial T}{\partial z}\right)_{b^-} - \kappa\left(\frac{\partial T}{\partial z}\right)_{b^+}, \tag{2.3c}$$

$$C_b\,(1-\chi_b)\,\dot{b} = D\chi_b\left(\frac{\partial C}{\partial z}\right)_{b^-} - D\left(\frac{\partial C}{\partial z}\right)_{b^+}, \tag{2.3d}$$

$$\left(\frac{\partial T}{\partial z}\right)_{+} = -\Gamma\left(\frac{\partial C}{\partial z}\right)_{+}. \tag{2.3e}$$

The third condition is a Stefan condition balancing heat flux with the release of latent heat, and the fourth is a Stefan condition balancing solute flux with solute rejection. The fifth condition is a condition of marginal equilibrium, introduced by Worster (1986), describing the minimum thermal gradient at the interface which would not result in further growth of the mush. As shown in Worster (1986), the assumption of equal thermal properties in all phases allows this fifth condition to be replaced by the condition

$$\chi_b = 1, \tag{2.3f}$$

which simplifies (2.3*c*) and (2.3*d*).

In the mush, $a(t) < z < b(t)$,

$$\frac{\partial T}{\partial t} = \kappa\frac{\partial^2 T}{\partial z^2} - \frac{L}{c_p}\frac{\partial \chi}{\partial t}, \tag{2.4a}$$

$$\frac{\partial(\chi C)}{\partial t} = D\frac{\partial}{\partial z}\left(\chi\frac{\partial C}{\partial z}\right), \tag{2.4b}$$

$$T = T_M - \Gamma C, \tag{2.4c}$$

where L is the latent heat per unit mass, ρ is the density, c_p is the specific heat per unit mass, χ is the liquid fraction, Γ is the slope of the liquidus, which is assumed to be linear, and T_M is the melting temperature of the pure material. The third equation is an approximation of the liquidus curve, and represents local thermal equilibrium within the mush. The underlying assumption is that dendrites grow or decay sufficiently to maintain this relationship.

At the solid–mush interface, $z = a(t)$,

$$[T]_{-}^{+} = 0, \tag{2.5a}$$

$$\frac{L}{c_p}\chi_a\dot{a} = \kappa\left(\frac{\partial T}{\partial z}\right)_{a^-} - \kappa\left(\frac{\partial T}{\partial z}\right)_{a^+}, \tag{2.5b}$$

$$C_a\chi_a\dot{a} = -D\chi_a\left(\frac{\partial C}{\partial z}\right)_{a^+}. \tag{2.5c}$$

The second and third conditions serve the same roles at this interface as (2.3*c*) and (2.3*d*) serve at the mush–liquid interface.

In the solid, $0 < z < a(t)$,

$$\frac{\partial T}{\partial t} = \kappa\frac{\partial^2 T}{\partial z^2}, \tag{2.6a}$$

https://doi.org/10.1017/jfm.2011.420 Published online by Cambridge University Press

$$\frac{\partial \mathscr{C}}{\partial t} = 0, \tag{2.6b}$$

where $\mathscr{C}$ denotes the locally averaged concentration in the solid phase. In the case of a non-eutectic solid–mush interface with our assumption of complete solute rejection, we have $\mathscr{C} = 0$. This will change in the eutectic case, however.

At the bottom of the tank, $z = 0$,

$$T = T_B. \tag{2.7}$$

The initial conditions for this system are

$$T(z, 0) = T_\infty, \tag{2.8a}$$

$$C(z, 0) = C_0. \tag{2.8b}$$

This system produces a solid–mush interface satisfying $\mathscr{C} = 0$. If $T_B < T_E$, it is possible that the solid–mush interface will have a temperature below the eutectic, so a eutectic front would appear instead, which is the possibility specifically studied by Anderson (2003). Such a possibility was also accounted for in the models of Fowler (1985) and Emms & Fowler (1994). In this case, we replace (2.5*a*)–(2.5*c*) with

$$[T]^+_- = 0, \tag{2.9a}$$

$$T = T_E, \tag{2.9b}$$

$$\frac{L}{c_p}\chi_a \dot{a} = \kappa \left(\frac{\partial T}{\partial z}\right)_{a^-} - \kappa \left(\frac{\partial T}{\partial z}\right)_{a^+}, \tag{2.9c}$$

$$(\mathscr{C}_{a^-} - C_{a^+}\chi_{a^+})\,\dot{a} = D\chi_{a^+}\left(\frac{\partial C}{\partial z}\right)_{a^+}. \tag{2.9d}$$

The concentration of solute that is frozen into the solid is given by $\mathscr{C}_{a^-}$, an unknown quantity which must be determined by (2.9*d*). We will assume that there is no solute diffusion within the solid. Since the concentration in the mushy layer is tied to temperature through the liquidus relationship (2.4*c*), the second condition above can also be expressed as

$$C_{a^+} = C_E. \tag{2.10}$$

3. Similarity solutions

The systems set forth in the previous section admit similarity solutions, specifically through the similarity variable

$$\eta = \frac{z}{\sqrt{4\kappa t}}, \tag{3.1}$$

with the mush–liquid and solid–mush interfaces respectively satisfying

$$b(t) = 2\lambda_b\sqrt{\kappa t}, \tag{3.2a}$$

$$a(t) = 2\lambda_a\sqrt{\kappa t}. \tag{3.2b}$$

This transforms the system from a system of partial differential equations to a system of ordinary differential equations. The details of the similarity solutions in the two cases under consideration can be determined by modifications of Worster (1986) and Anderson (2003). Under the assumption of complete solute rejection from non-eutectic solid, as in both of those studies, the similarity solution with a non-eutectic solid–mush interface has no solute frozen into the solid, and the similarity

https://doi.org/10.1017/jfm.2011.420 Published online by Cambridge University Press

solution with a eutectic solid–mush interface has a constant non-zero quantity of solute being frozen in for all time. Additionally, in the case of a non-eutectic interface, the interface follows an isotherm with $T > T_E$, but the eutectic interface follows the $T = T_E$ isotherm. As a result, only one of the similarity solutions will apply for a given set of parameters.

For the rest of this paper, we will assume negligible latent heat, so $L = 0$. In this case, the temperature profile for the similarity solutions is given by

$$T(\eta) = T_B + (T_\infty - T_B)\mathrm{erf}(\eta), \tag{3.3}$$

where $\mathrm{erf}(\eta)$ is the error function

$$\mathrm{erf}(\eta) = \frac{2}{\sqrt{\pi}} \int_0^\eta \mathrm{e}^{-\xi^2}\, \mathrm{d}\xi. \tag{3.4}$$

We will also use the complementary error function, $\mathrm{erfc}(\eta) = 1 - \mathrm{erf}(\eta)$. For the similarity solution which satisfies (2.5*a*)–(2.5*c*), which has a non-eutectic solid–mush interface, we have

$$C(\eta) = \begin{cases} C_0 + \dfrac{(C_h - C_0)\mathrm{erfc}\left(\eta/\sqrt{\epsilon}\right)}{\mathrm{erfc}\left(\lambda_b/\sqrt{\epsilon}\right)}, & \lambda_b < \eta, \\ (T_M - T(\eta))/\Gamma, & \lambda_a < \eta < \lambda_b, \\ 0, & 0 < \eta < \lambda_a, \end{cases} \tag{3.5}$$

and

$$\mathscr{C}(\eta) \equiv 0, \tag{3.6}$$

where λ_b and λ_a satisfy

$$\exp\left(\left(\frac{1}{\epsilon} - 1\right)\lambda_b^2\right) = \frac{-\Gamma C_0 - T_B - (T_\infty - T_B)\mathrm{erf}(\lambda_b)}{\sqrt{\epsilon}(T_\infty - T_B)\mathrm{erfc}\left(\lambda_b/\sqrt{\epsilon}\right)}, \tag{3.7a}$$

$$0 = \left(2\lambda_a C_{a^+} + \epsilon C'_{a^+}\right)\chi_{a^+}, \tag{3.7b}$$

with $\epsilon = D/\kappa$. The derivative of C with respect to the similarity variable η is denoted by C'. We note that (3.7*b*) requires either

$$\chi_{a^+} = 0 \tag{3.8a}$$

or

$$2\lambda_a C_{a^+} + \epsilon C'_{a^+} = 0, \tag{3.8b}$$

but we will demonstrate at the end of this section that both of these conditions are satisfied, which is guaranteed only when latent heat is neglected.

For the similarity solution with a eutectic solid–mush front,

$$C(\eta) = \begin{cases} C_0 + \dfrac{(C_h - C_0)\mathrm{erfc}\left(\eta/\sqrt{\epsilon}\right)}{\mathrm{erfc}\left(\lambda_b/\sqrt{\epsilon}\right)}, & \lambda_b < \eta, \\ (T_M - T(\eta))/\Gamma, & \lambda_E < \eta < \lambda_b, \\ 0, & 0 < \eta < \lambda_E, \end{cases} \tag{3.9}$$

and

$$\mathscr{C}(\eta) = \begin{cases} 0, & \lambda_E < \eta, \\ \mathscr{C}_{a^-}, & 0 < \eta < \lambda_E, \end{cases} \tag{3.10}$$

https://doi.org/10.1017/jfm.2011.420 Published online by Cambridge University Press

where λ_b satisfies (3.7*a*) and λ_E solves

$$\mathrm{erf}(\lambda_E) = (T_E - T_B)/(T_\infty - T_B). \tag{3.11a}$$

For both similarity solutions, the liquid fraction is given by

$$\chi(\eta) = \chi_b \exp\left(\int_\eta^{\lambda_b} \frac{\epsilon C''(\xi) + 2\xi C'(\xi)}{\epsilon C'(\xi) + 2\xi C(\xi)}\,\mathrm{d}\xi\right), \tag{3.12}$$

where $\chi_b = 1$ due to the combination of our assumptions and the condition of marginal equilibrium.

We will now demonstrate that both of the conditions (3.8*a*) and (3.8*b*) are satisfied at the non-eutectic solid–mush interface. This is a summary of the discussion in theappendix of Gewecke & Schulze (2011). Under the given similarity transformation, the equation governing the liquid fraction in the mushy layer is

$$(2\eta C + \epsilon C')\chi' = -(2\eta C' + \epsilon C'')\chi. \tag{3.13}$$

When this is integrated, we get (3.12). The solid–mush interface position solves (3.7*b*). Now, if (3.8*b*) is satisfied, then the interface appears at a regular singular point of (3.13). Near the singularity, a series solution of the form

$$\chi(\eta) = \sum_{n=0}^{\infty} a_n (\eta - \xi_s)^{n+r} \tag{3.14}$$

can be identified if the function

$$p(\eta) = \frac{2\eta C' + \epsilon C''}{2\eta C + \epsilon C'} \tag{3.15}$$

has a simple pole at the singularity, which we denote ξ_s. This is indeed the case, and we find that

$$r = -\lim_{\eta\to\xi_s} (\eta - \xi_s)p(\eta) = \frac{-2(1-\epsilon)\xi_s^2}{2(1-\epsilon)\xi_s^2 - \epsilon}, \tag{3.16}$$

for the series solution. As a result, we find that

$$\chi_{a^+} = \lim_{\eta\to\lambda_a^+} \chi(\eta) = 0, \tag{3.17}$$

which satisfies (3.8*a*). On the other hand, if (3.8*a*) is satisfied but not (3.8*b*), then $\chi \equiv 0$ throughout the mushy layer, which contradicts $\chi_{b^-} = 1$. As a result, both of (3.8*a*) and (3.8*b*) are simultaneously satisfied when fulfilling (3.7*b*).

4. Switching temperature

It is natural to wonder which of the two sets of solid–mush interface conditions, (2.5*a*)–(2.5*c*) or (2.9*a*)–(2.9*d*), applies for a given set of parameters. If $T_B \geqslant T_E$ then the first case applies, and if $T_B \ll T_E$ then the second case applies, but for T_B below but near T_E there is some ambiguity. However, under the assumption of negligible latent heat, the main changes in the outcomes are the location of the solid–mush interface and the concentration on the solid side of that interface. The temperature profile in the whole domain, the mush–liquid interface position, and the concentration profile in the liquid remain the same, while the liquid fraction in the mushy layer is described by (3.12) despite the change in size of the resulting layer.

https://doi.org/10.1017/jfm.2011.420 Published online by Cambridge University Press

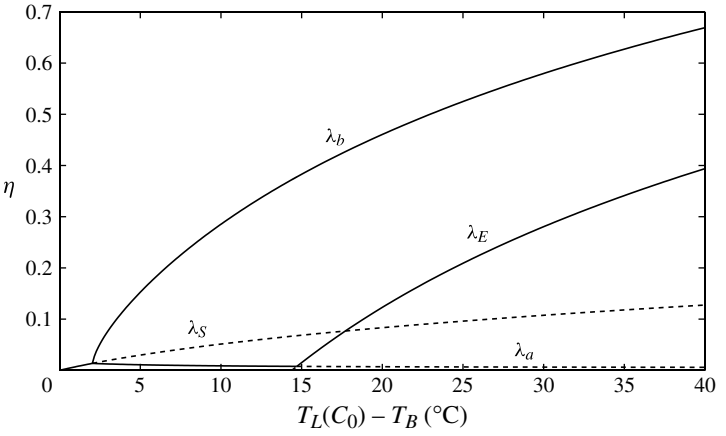


FIGURE 1. The various interface positions are shown as functions of the difference $T_L(C_0) - T_B$. The dashed curves represent the locations of interfaces that do not appear for a given temperature T_B. The λ values are in terms of the similarity variable. Here, λ_S is the solid–liquid interface position predicted by the Stefan problem, λ_a is the predicted non-eutectic solid–mush interface position, λ_b is the mush–liquid interface position, and λ_E is the location of the eutectic isotherm, which also corresponds to the predicted eutectic solid–mush interface position.

In figure 1 we demonstrate the predicted positions of the interface positions λ_i in terms of the similarity variable. For T_B near $T_L(C_0)$, only a liquid–solid interface appears. Once T_B is sufficiently cold for undercooling to occur at a solid–liquid interface, two interfaces bounding a mushy layer appear instead. For $T_B < T_E$, the eutectic solid–mush interface can be predicted, but the non-eutectic interface dominates for a relatively narrow range of T_B values. However, once T_B crosses some critical value T_B^*, the eutectic solid–mush front begins to dominate the non-eutectic solid–mush front. The left-hand portion of this figure, before the λ_E curve appears, is very similar to figure 5 in Worster (1986).

In the absence of any other method for determining which of the two conditions will hold for a given set of parameters, one could determine the similarity solution with a non-eutectic solid–mush interface and then check the temperature at the solid–mush interface. If that temperature were at or above the eutectic, then the correct system was used. If that temperature is instead below the eutectic, then the other system must be utilized. Rather than use this approach, it would be useful to have a method to determine *a priori* which of the two similarity solutions to use. We will present a method that fixes all parameters except for the temperature at the base of the tank T_B, and then determines the critical temperature T_B^* at which the switch between the two similarity solutions occurs.

We focus on the solid–mush boundary conditions. Under the assumption of negligible latent heat, these become

$$[T]_-^+ = 0, \tag{4.1a}$$

$$\left[\frac{\partial T}{\partial z}\right]_-^+ = 0, \tag{4.1b}$$

$$C_a \chi_a \dot{a} = -D\chi_a \left(\frac{\partial C}{\partial z}\right)_{a^+} \tag{4.1c}$$

https://doi.org/10.1017/jfm.2011.420 Published online by Cambridge University Press

for the non-eutectic front, and

$$[T]^{+}_{-} = 0, \tag{4.2a}$$

$$T = T_E, \tag{4.2b}$$

$$C = C_E, \tag{4.2c}$$

$$\left[\frac{\partial T}{\partial z}\right]^{+}_{-} = 0, \tag{4.2d}$$

$$(\mathscr{C}_{a^-} - C_{a^+}\chi_{a^+})\,\dot{a} = D\chi_{a^+}\left(\frac{\partial C}{\partial z}\right)_{a^+} \tag{4.2e}$$

for the eutectic front. Should the two fronts coincide, we find by combining (4.1*c*) and (4.2*e*) that

$$\mathscr{C}_{a^-} = 0, \tag{4.3}$$

which is expected for the non-eutectic front.

For both systems, we know that the temperature field is given by (3.3). In terms of the similarity variable, (4.1*c*) becomes

$$\left(C_{a^+} + \frac{\epsilon}{2\lambda_a}C'_{a^+}\right)\chi_{a^+} = 0 \tag{4.4}$$

for a non-eutectic front, and (4.2*e*) becomes

$$\left(C_E + \frac{\epsilon}{2\lambda_a}C'_{a^+}\right)\chi_{a^+} = \mathscr{C}_{a^-} \tag{4.5}$$

for a eutectic front, where C' denotes the derivative of concentration with respect to η. Furthermore, in the diffusion-controlled case,

$$\chi_{a^+} = 0, \tag{4.6}$$

$$C_{a^+} + \frac{\epsilon}{2\lambda_{a^+}}C'_{a^+} = 0 \tag{4.7}$$

both hold, as previously discussed in § 3. Assuming that the two fronts coincide, we can combine the conditions above to find that

$$C_E + \frac{\epsilon}{2\lambda_a}C'_{a^+} = 0, \tag{4.8}$$

where

$$\mathrm{erf}(\lambda_a) = \frac{T_E - T_B}{T_\infty - T_B}. \tag{4.9}$$

Alternatively, we can manipulate (4.8) and utilize the liquidus relationship (2.4*c*) to get the switching condition

$$2\lambda_a(T_E - T_M) + \epsilon T'_{a^+} = 0. \tag{4.10}$$

As a result, we can fix all but one of the parameters and determine the critical value of the remaining parameter which causes the switch in the conditions at the interface. Realistically, since κ, D, T_E, C_E, and Γ are fixed for a given material, and since C_0 is not present in the above condition, we can fix T_∞ and determine the critical temperature T_B at the base of the tank which causes the switch, or we can fix T_B and determine the critical initial and far-field temperature T_∞.

https://doi.org/10.1017/jfm.2011.420 Published online by Cambridge University Press

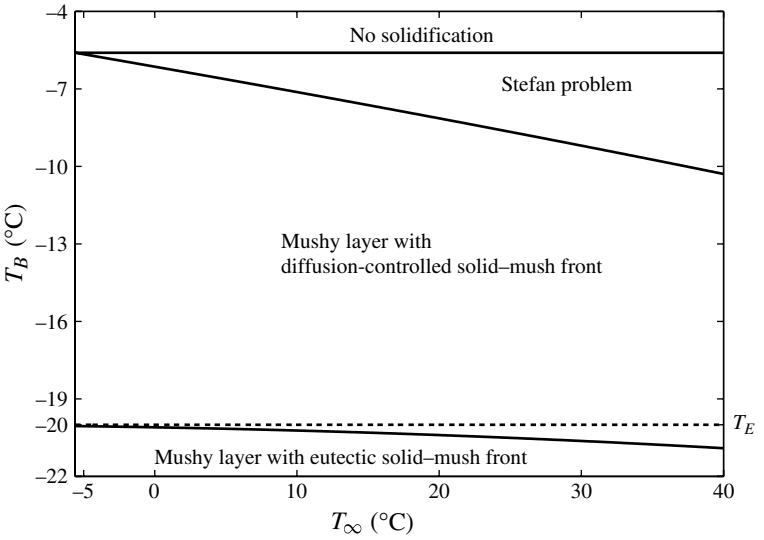


FIGURE 2. The horizontal line near the top indicates the maximum temperature at the bottom of the tank T_B at which solidification will occur, and is at $T_B = T_L(C_0)$. The middle curve describes the critical temperature at the bottom of the tank at which a mushy layer first appears. The lower curve describes the critical temperature at the bottom of the tank at which the solid–mush front transitions to a eutectic front. In other words, the three curves divide the T_∞–T_B plane into four regions: a region at the top where no solidification occurs, the upper-middle region where a solid–liquid front appears, the lower-middle region where a mushy layer appears with a non-eutectic solid–mush front, and the lower region where a mushy layer appears with a eutectic solid–mush front. The dashed line at $T_B = T_E = -20$ is shown as a reference point for comparison with the lower curve.

To determine the critical value T_B^* numerically, we perform a Newton iteration on (4.10), which incorporates (4.9). For temperatures T_B at the base of the tank below this critical value, the eutectic solid–mush front will appear. Otherwise, the non-eutectic front will appear. A similar routine can be used to calculate a critical value of T_∞^* given T_B. In figure 2 we show a portion of the T_∞–T_B plane separated into four regions, one where no solidification occurs, one where there is no mush, one where the non-eutectic solid–mush front appears, and one where the eutectic solid–mush front appears. For these purposes, we have utilized the parameters of Set I from Table 1 in Worster (1986), which roughly approximate a 14 % sodium nitrate solution, with latent heat omitted.

5. Finite-domain case

For a finite domain, only a few modifications to the model are required. Instead of far-field conditions, we instead have at an upper boundary $z = H$ the conditions

$$T = T_H, \tag{5.1a}$$

$$\frac{\partial C}{\partial z} = 0, \tag{5.1b}$$

where $T_H > T_L(C_0)$. The first condition states that the temperature at the top of the tank is fixed, and the second states that no solute may exit the tank. Additionally, the

https://doi.org/10.1017/jfm.2011.420 Published online by Cambridge University Press

initial conditions are

$$T(z,0) = T_H, \tag{5.2a}$$

$$C(z,0) = C_0. \tag{5.2b}$$

We have delayed introduction of a rescaled system until this point because the infinite-domain system lacks a clear choice of length scale, whereas the finite-domain system has the natural length scale H. We non-dimensionalize both systems using the scalings

$$\theta = \frac{T - T_E}{T_H - T_E}, \quad \hat{t} = \frac{\kappa}{H^2}t, \quad \hat{z} = \frac{1}{H}z. \tag{5.3}$$

The concentration C is scaled so that it ranges between zero and one, but with the eutectic concentration C_E satisfying $0 < C_E < 1$. These scalings are the same as those used by Gewecke & Schulze (2011), but with a modified thermal scaling. Non-dimensional parameters will be presented as they arise, but we note that the Stefan number will not appear due to our standing assumption of negligible latent heat. We will also drop the 'hats' on the variables, so any references to these variables will refer to the non-dimensional variables unless otherwise noted.

The boundary conditions at the upper boundary (now $z = 1$) become

$$\theta = 1, \tag{5.4a}$$

$$\frac{\partial C}{\partial z} = 0. \tag{5.4b}$$

In the liquid region $b(t) < z < 1$ the equations become

$$\frac{\partial \theta}{\partial t} = \frac{\partial^2 \theta}{\partial z^2}, \tag{5.5a}$$

$$\frac{\partial C}{\partial t} = \epsilon \frac{\partial^2 C}{\partial z^2}, \tag{5.5b}$$

where $\epsilon = D/\kappa$ is the inverse Lewis number.

At the mush–liquid interface $z = b(t)$ the conditions become

$$[\theta]^+_- = 0, \tag{5.6a}$$

$$[C]^+_- = 0, \tag{5.6b}$$

$$\left[\frac{\partial \theta}{\partial z}\right]^+_- = 0, \tag{5.6c}$$

$$C_b(1 - \chi_b)\dot{b} = \epsilon \chi_b \left(\frac{\partial C}{\partial z}\right)_{b^-} - \epsilon \left(\frac{\partial C}{\partial z}\right)_{b^+}. \tag{5.6d}$$

The condition of marginal equilibrium given by Worster (1986), which in the present case takes the form

$$\chi(b^-(t), t) = \chi_{b^-} = 1, \tag{5.7a}$$

applies whenever

$$\dot{b}(t) > -\epsilon \left(\frac{\partial C}{\partial z}(b^-(t), t)\right) \Big/ C(b^-(t), t). \tag{5.7b}$$

This specifies a value for χ_b only when such a condition is needed, which is when the interface is advancing more rapidly than the leading characteristic. Otherwise, the

https://doi.org/10.1017/jfm.2011.420 Published online by Cambridge University Press

value of χ_b is determined by the characteristic curves terminating on the interface. This restriction indicating when the condition of marginal equilibrium applies was identified in Gewecke & Schulze (2011). The condition of marginal equilibrium reflects the idea that the mushy layer grows to resolve undercooling, and this condition should not be expected to hold when there is no undercooling to relieve. In the latter case, the diffusion of solute from the mushy layer into the liquid layer controls the evolution of the interface. In general, the condition of marginal equilibrium will cause $0 < \chi_b \leqslant 1$ whenever that condition applies.

In the mushy layer $a(t) < z < b(t)$ the equations become

$$\frac{\partial \theta}{\partial t} = \frac{\partial^2 \theta}{\partial z^2}, \tag{5.8a}$$

$$\frac{\partial (\chi C)}{\partial t} = \epsilon \frac{\partial}{\partial z}\left(\chi \frac{\partial C}{\partial z}\right), \tag{5.8b}$$

$$\theta = -\hat{\Gamma}(C - C_E), \tag{5.8c}$$

where $\hat{\Gamma} = \Gamma/(T_H - T_E)$.

At the solid–mush interface $z = a(t)$ the conditions depend upon whether the interface is eutectic or non-eutectic. They can be summarized, similar to Fowler (1985) and Emms & Fowler (1994), as

$$\begin{cases} \theta = 0 & \text{(eutectic)}, \\ \mathscr{C}_{a^-} = 0 & \text{(non-eutectic)}, \end{cases} \tag{5.9a}$$

$$[\theta]^+_- = 0, \tag{5.9b}$$

$$\left[\frac{\partial \theta}{\partial z}\right]^+_- = 0, \tag{5.9c}$$

$$(\mathscr{C}_{a^-} - C_{a^+}\chi_{a^+})\,\dot{a} = \epsilon \chi_{a^+}\left(\frac{\partial C}{\partial z}\right)_{a^+}. \tag{5.9d}$$

As in Gewecke & Schulze (2011), the thermal field is independent of the concentration and liquid fraction due to negligible latent heat. Additionally, the liquid fraction in the mush can be tracked by the method of characteristics. The characteristic curves initiate on the mush–liquid interface but eventually terminate along either the mush–liquid interface or the solid–mush interface. The position of the characteristics and the liquid fraction along such characteristics is described by

$$\dot{\zeta}(s) = -\epsilon \left(\frac{\partial C}{\partial z}(\zeta(s), \tau(s))\right) \Big/ C(\zeta(s), \tau(s)), \tag{5.10a}$$

$$\dot{\tau}(s) = 1, \tag{5.10b}$$

$$\chi(s) = \exp\left(\int_0^s \frac{\epsilon \dfrac{\partial^2 C}{\partial z^2}(\zeta(\xi), \tau(\xi)) - \dfrac{\partial C}{\partial t}(\zeta(\xi), \tau(\xi))}{C(\zeta(\xi), \tau(\xi))}\,\mathrm{d}\xi\right). \tag{5.10c}$$

This leads to the condition described by (5.7*a*,*b*). The evolution of characteristic curves is illustrated in figure 3. The solid–mush interface advances more rapidly than characteristics initiated at early times, but eventually slows to follow a characteristic, when the front becomes diffusion-controlled instead of eutectic.

https://doi.org/10.1017/jfm.2011.420 Published online by Cambridge University Press

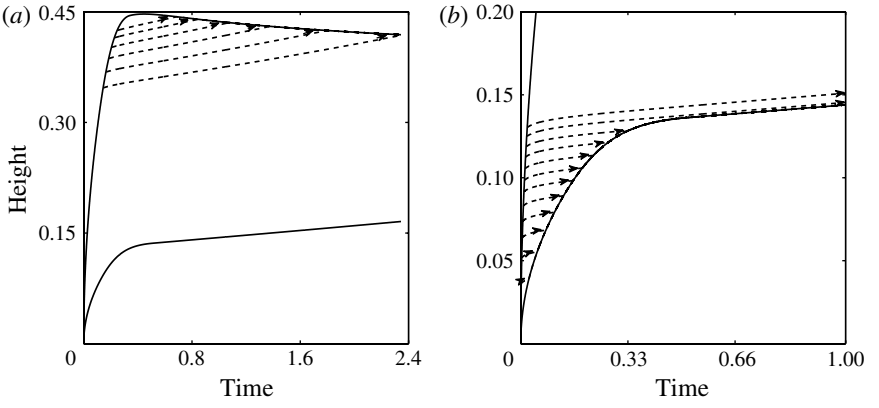


FIGURE 3. Characteristic curves (dashed) initiate along the mush–liquid interface (upper solid curve), and (*a*) terminate on the mush–liquid interface as in Gewecke & Schulze (2011) or (*b*) along a eutectic solid–mush interface (lower solid curve). Once the solid–mush interface switches from eutectic to diffusion-controlled, the interface follows a characteristic. This can be seen in (*b*).

Additionally, this description of the characteristics allows us to recast the condition (5.9*a*) at the solid–mush interface as

$$\begin{cases} \theta = 0 & \text{when } \dot{a} > -\epsilon \left(\dfrac{\partial C}{\partial z}(a^+(t), t) \right) \Big/ C(a^+(t), t), \\ \mathscr{C}_{a^-} = 0 & \text{otherwise.} \end{cases} \tag{5.11}$$

Alternatively, we may use $C_{a^+} = C_E$ instead of $\theta = 0$, due to the liquidus relationship.

6. Numerical method

Our numerical scheme modifies the scheme presented in Gewecke & Schulze (2011), accounting for the possibility of a eutectic solid–mush front. An additional quantity, the concentration in the solid region, must be calculated and retained. Since the system will be initialized using the similarity solutions, we must determine which of the two similarity solutions to use, as discussed in § 4. At each time step, care must be taken to find the correct solid–mush interface, whether it be a eutectic or a non-eutectic front.

The discretizations are much the same as in Gewecke & Schulze (2011), but we will give a brief overview below. We will then discuss the numerical method, explaining how each quantity is determined.

6.1. *Discretization*

The various quantities in this problem appear on different domains. As a result, the discretizations for each quantity are different. To transfer data between different computational grids, we interpolate data as needed.

The liquid fraction is only computed within the mushy zone. Since we track the liquid fraction along characteristic curves, there is no fixed computational grid nor is there uniform spacing. The temperature field, since it is not influenced by any other quantities in the problem, uses a uniform spatial discretization over the full domain.

The concentration is handled separately in each of the three subdomains. In the solid layer, we keep track of the concentration on the solid side of the solid–mush interface

https://doi.org/10.1017/jfm.2011.420 Published online by Cambridge University Press

at each time step, and that quantity becomes frozen in, so at any given time, the concentration in the solid can be determined by that data. There is no solute diffusion within the solid, so there is no specific computational grid needed. The history of the solid–mush interface position dictates the spatial grid within the solid. In the mushy layer, the concentration and its derivatives can at all times be computed from the temperature field through use of the liquidus relationship. For the liquid layer, we utilize the mapping

$$\tau = t, \quad \xi = \frac{z - b(t)}{1 - b(t)} \tag{6.1}$$

from $(b(t), 1)$ to $(0, 1)$. This transformation changes (5.5*b*) into

$$\frac{\partial C}{\partial \tau} - \frac{(1-\xi)\dot{b}(\tau)}{H - b(\tau)} \frac{\partial C}{\partial \xi} = \frac{\epsilon}{(H - b(\tau))^2} \frac{\partial^2 C}{\partial \xi^2}. \tag{6.2}$$

The gridpoints in $(0, 1)$ do not move, so data at the previous time step can be utilized directly.

6.2. *Scheme*

We initialize the system at some very small initial time t_s using one of the two similarity solutions. To pick between the two, we calculate the switching temperature T_B^* using the method outlined earlier and compare with our prescribed value of T_B. A small number of characteristics are initiated at this time, including a characteristic at each of the two interfaces.

For each following time step t_i, we do the following.

(*a*) We update the temperature distribution over the whole domain.

(*b*) For each characteristic present at t_{i-1}, we update the position and liquid fraction data, assuming that all characteristics remain in the mush. The values for concentration and its derivatives are calculated using the liquidus relationship and interpolating the values of θ and its derivatives.

(*c*) We determine the location of the solid–mush interface a_i. Since the non-eutectic solid–mush interface follows a characteristic, we first check to see if the corresponding characteristic has temperature above or below T_E. If it is above that temperature, then we accept that position as the interface position, set the concentration on the solid side of the interface to zero, and proceed to the next step. If the temperature is instead at or below the eutectic, we perform the following steps.

  (i) Perform a search to identify the position of the $T = T_E$ isotherm. This position will be a_i.

  (ii) The liquid fraction on the mush side of the interface is determined by the characteristics terminating on the interface.

  (iii) We calculate the concentration on the solid side of the interface, using (5.9*d*).

  (iv) The characteristics which terminated along the solid–mush interface, which are those whose positions had been calculated to be below the new interface position, are removed. In practice, the locations of these characteristics and the liquid fraction along these characteristics are set to the values at the interface.

(*d*) We then determine the location of the mush–liquid interface b_i.

  (i) We guess an interface position b_i and a secondary guess $b_i + \delta$, with δ small.

https://doi.org/10.1017/jfm.2011.420 Published online by Cambridge University Press

(ii) The concentration field in the liquid is calculated using the two guess values above.

(iii) Residuals for each of the two guesses are calculated using (5.6*d*).

(iv) Using the residuals calculated in the previous step, we use a secant-line approximation of the derivative in a Newton iteration to update the guess for b_i. With this updated guess, we repeat the previous two steps.

(v) Once the size in the change for the guess is small enough, we terminate the iteration. If the accepted value of b_i is ahead of the leading characteristic, we initialize a characteristic at (b_i, t_i) with $\chi = 1$. If the accepted value of b_i is not ahead of the leading characteristic, we remove characteristics as needed so that the leading characteristic is at (t_i, b_i). In practice, the locations of such characteristics and their corresponding liquid fractions are set to the values at the interface. We then proceed to the next time step.

7. Results

The parameters used to produce results are from Set I of Table 1 in Worster (1986), with some slight modifications due to treating the concentration as a fraction rather than a percentage. Additionally, we set $C_E = 0.5$ and $T_E = -20$ °C, primarily for convenience. These parameters roughly approximate a 14 % sodium nitrate solution. Set II of Table 1 in Worster (1986) more accurately represents such a solution, but does not exhibit equal thermal properties in all phases. We additionally set $T_H = 15$ °C and $T_B = -25.6$ °C, with the height of the tank being $H = 15$ cm. In non-dimensional terms, we have $\epsilon \approx 7.7 \times 10^{-3}$, $\hat{\Gamma} \approx 1.143$, $\theta_B = -0.16$, and the melting temperature of the pure material $T_M = 0$ corresponds to $\theta \approx 0.57$.

In figure 4 the positions of the solid–mush and mush–liquid interfaces are plotted against time, with a circle indicating where the solid–mush interface switches type. Figure 4(*a*) demonstrates the evolution until the mush vanishes, whereas figure 4(*b*) shows the evolution over a longer range of time values, with a solid–liquid front present after the mushy layer has vanished. Over a short time, both of the interfaces advance very rapidly, but each eventually slows. After a critical time, the solid–mush interface switches from a eutectic front to a diffusion-controlled interface, which continues to advance until the disappearance of the mushy layer.

There are two natural time scales for this system, namely the thermal diffusivity time scale H^2/κ and the solute diffusivity time scale H^2/D. The advance of the mushy layer is on the thermal time scale and the approach to the eventual steady state is on the solutal time scale. While the disappearance of the mushy layer relies upon the presence of solute diffusion, the precise time scale of this effect relies upon the maximal thickness of the mushy layer rather than the full depth of the tank.

We demonstrate the evolution of the concentration profile in figure 5. Below the solid–mush interface the concentration of solute frozen into the solid is shown, and above the interface the concentration in the liquid phase is shown. We have already demonstrated in figure 4 that the solid–mush front never retreats, so the solute that is frozen into the solid at the interface remains in the same place forever. Figure 5(*a*) shows the concentration profile at an instant when the solid–mush interface is eutectic, figure 5(*b*) shows the concentration profile at the instant when the solid–mush interface changes type, and figure 5(*c*) shows the concentration at a later time when a small region of pure solid can be seen. The concentration on the solid side of the interface is plotted as a function of time in figure 6, to highlight the fact that the amount of solute being frozen into the solid declines over time, eventually becoming negligible

https://doi.org/10.1017/jfm.2011.420 Published online by Cambridge University Press

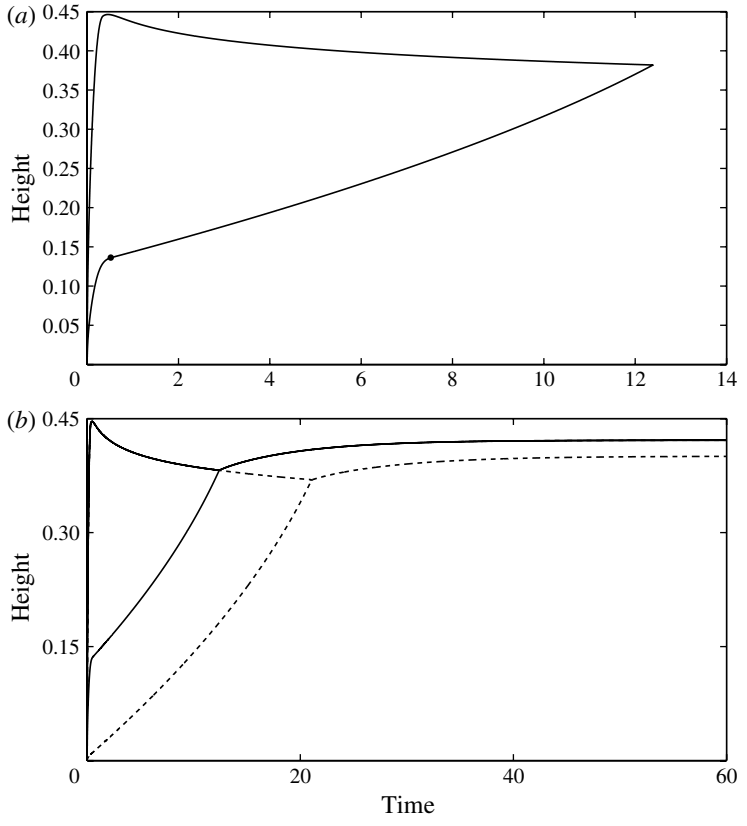


FIGURE 4. (*a*) The solid–mush (lower curve) and mush–liquid (upper curve) interface positions from $t = 0$ to the time when the mush vanishes. The circle on the solid–mush curve indicates the time at which the front changes from eutectic to non-eutectic. (*b*) The long-time behaviour, with only a single curve denoting the solid–liquid interface once the mush has vanished. The dashed curves in (*b*) indicate the behaviour if the eutectic effects are ignored. The parameters used are provided in the main text.

once the evolution of the temperature field has stagnated sufficiently. Once that occurs, the solid–mush front switches from a eutectic front to a non-eutectic front.

The evolution of the liquid fraction in the mushy zone is given in figure 7. Early on, the liquid fraction appears to behave as in the similarity solution, as the profile mainly gets stretched out. Once the temperature field has equilibrated, the liquid fraction along each characteristic is constant, so the curve advances with the characteristics, with portions of the curve vanishing as characteristics pass the mush–liquid interface. This behaviour is similar to that exhibited by the case where only non-eutectic solid forms, as in Gewecke & Schulze (2011), with one major difference. In the absence of latent heat, the liquid fraction on the mush side of the solid–mush interface drops to zero when no eutectic solid forms. In the present case, the liquid fraction does not decay to zero on the mush side of the interface, even after non-eutectic solid begins to form.

Another important aspect is how this solution compares with the solution that would be generated if we were to ignore the possibility of a $T = T_E$ front. Figure 4(*b*) shows the interface positions generated in the present case along with the interface positions

https://doi.org/10.1017/jfm.2011.420 Published online by Cambridge University Press

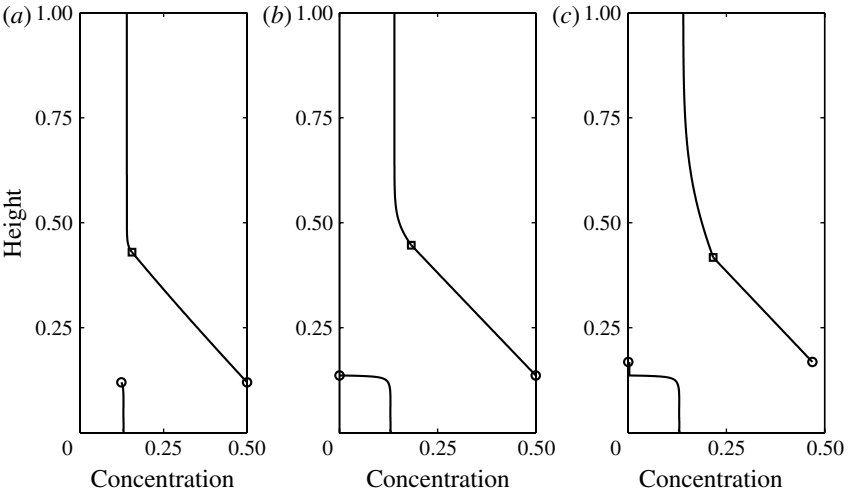


FIGURE 5. Three different snapshots of the concentration profile. The circles in each image represent the location of the solid–mush interface; note the jump in concentration across the interface. The square in each image represents the location of the mush–liquid interface. In (*a*) we see a sample concentration profile while the eutectic solid–mush front is present. In (*b*) we see the concentration profile when the transition from eutectic to non-eutectic solid–mush interface occurs. The concentration profile at a later time is shown in (*c*), where the jump in the concentration gradient at the mush–liquid interface is visible.

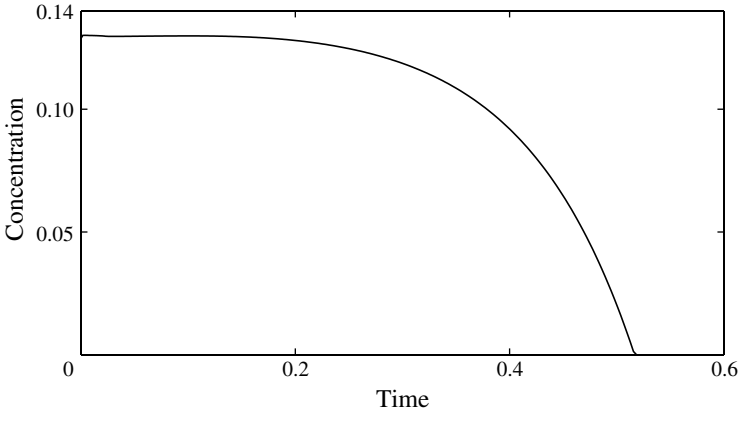


FIGURE 6. As time progresses, the concentration frozen in at the solid–mush interface varies. This corresponds to the variation through the solid layer demonstrated in figure 5.

generated by utilizing the method set forth in Gewecke & Schulze (2011), ignoring the impact of eutectics. We see three major impacts. The most easily predicted impact is that the solid–mush interface advances much more rapidly at early times when the $T = T_E$ front is incorporated. Next, we see that the time until the mush vanishes is reduced. This is primarily due to the rapid advance of the solid–mush front at early times. Finally, we can see that the eventual steady states are different, with the solid–liquid interface advancing farther when the $T = T_E$ interface is incorporated. This is also an intuitive result, as some of the solute becomes incorporated in the solid, so

https://doi.org/10.1017/jfm.2011.420 Published online by Cambridge University Press

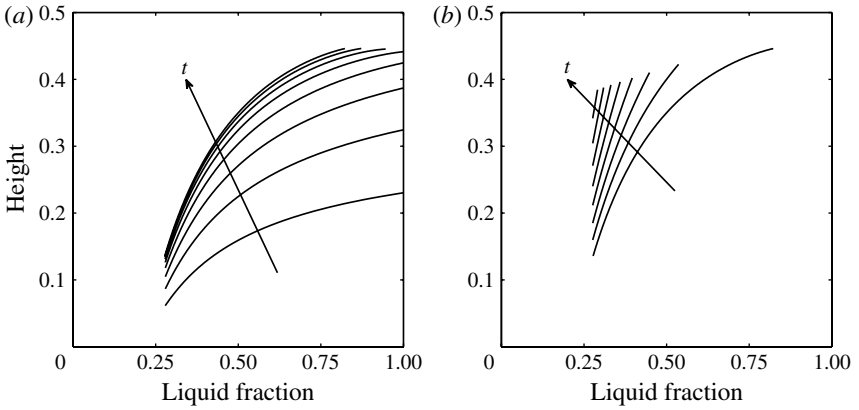


FIGURE 7. The curves are liquid fraction (χ) profiles within the mush at various stages of system evolution. The curves in (*a*) are at evenly spaced intervals during the advance of the mush–liquid interface. The remainder of the time until the mush vanishes is illustrated in (*b*), again at evenly spaced intervals.

there is less total solute in the liquid in this long-time regime. Since the steady-state location of the solid–liquid interface is dictated by the liquidus relationship, with the concentration being the uniform concentration of the remaining liquid, the interface must advance farther when less solute is present.

8. Conclusions

When a finite-height tank filled with a uniformly mixed binary alloy is placed onto a cold surface, a mushy layer may form. If it does form, the mushy layer initially advances very rapidly into the liquid region. A solid layer also grows, but the growth of the solid layer may be rapid or slow, depending upon the temperature at the base of the tank. If the cold surface is sufficiently cold, the solid–mush interface will initially be dictated by the isotherm associated with the eutectic temperature and will move rapidly, though not as rapidly as the mush–liquid interface. Once the advance of the isotherm slows, the advance of the solid–mush front will be dictated by solute diffusion, and this advance will be slow. If the cold surface is above some critical temperature, then the solid–mush front will advance slowly, as discussed in Gewecke & Schulze (2011). In either case, the mush–liquid interface eventually begins a very slow retreat. The solid–mush front continues its slow advance until it overtakes the mush–liquid interface, which takes a long time. After the mushy layer has been eliminated, a solid–liquid front progresses until the system stabilizes.

This switch between two different solid–mush interface types, eutectic and diffusion-controlled, is an important feature. In the case of an infinite domain, using our assumptions, we can identify the base temperature at which this switch occurs for a particular alloy. This also aids in identifying the early-time dynamics in the case of a finite tank, when the similarity solutions from the infinite domain serve as excellent approximations of the true solutions. In a finite tank, we get additional information when we recognize the presence of both conditions. If the solid–mush interface is a eutectic front at early times, then the amount of solute being frozen into the solid varies with time, which essentially writes a history of the system into the solid. Under our assumption of complete solute rejection, once the system equilibrates we will have

https://doi.org/10.1017/jfm.2011.420 Published online by Cambridge University Press

a liquid region in equilibrium with a heterogeneous solid region. This solid region will essentially have three layers: a bottom layer with a nearly uniform concentration of solute frozen in, a middle transition layer where the concentration of solute decays to zero, and then an upper layer that is pure, as can be seen in figure 5.

The variation of solute concentration within the solid is also of interest. The similarity solution for the infinite domain has uniform concentration throughout the solid, as does the solution for the finite domain with no solute diffusion. This may also have physical consequences, contributing to variations in the microstructure of the resulting solid. Following the discussion in Kerr *et al.* (1990), the eutectic solid that forms in the present case consists of frozen interstitial fluid (with concentration at the eutectic) between dendrites that were previously a part of the mushy layer. This variation of concentration in the solid phase may also have consequences in geophysical applications of mushy layers, such as the solidification of magma chambers.

Acknowledgements

We are grateful to D. M. Anderson for helpful discussions in the preliminary stages of this work. We would also like to acknowledge support from the National Science Foundation, through grant numbers DMS-0707443 and DMS-0854870.

REFERENCES

ANDERSON, D. M. 2003 A model for diffusion-controlled solidification of ternary alloys in mushy layers. *J. Fluid Mech.* **483**, 165–197.

DAVIS, S. H. 2001 *Theory of Solidification*. Cambridge University Press.

EMMS, P. W. & FOWLER, A. C. 1994 Compositional convection in the solidification of binary alloys. *J. Fluid Mech.* **262**, 111–139.

FOWLER, A. C. 1985 The formation of freckles in binary alloys. *IMA J. Appl. Math.* **35**, 159–174.

GEWECKE, N. R. & SCHULZE, T. P. 2011 The rapid advance and slow retreat of a mushy zone. *J. Fluid Mech.* **674**, 227–243.

KERR, R. C., WOODS, A. W., WORSTER, M. G. & HUPPERT, H. E. 1990 Solidification of an alloy cooled from above. Part 3. Compositional stratification within the solid. *J. Fluid Mech.* **218**, 337–354.

LANGER, J. S. 1980 Instabilities and pattern formation in crystal growth. *Rev. Mod. Phys.* **52**, 1–28.

SCHULZE, T. P. & WORSTER, M. G. 1999 Weak convection, liquid inclusions and the formation of chimneys in mushy layers. *J. Fluid Mech.* **388**, 197–215.

SCHULZE, T. P. & WORSTER, M. G. 2005 A time-dependent formulation of the mushy-zone free-boundary problem. *J. Fluid Mech.* **541**, 193–202.

WORSTER, M. G. 1986 Solidification of an alloy from a cooled boundary. *J. Fluid Mech.* **167**, 481–501.

https://doi.org/10.1017/jfm.2011.420 Published online by Cambridge University Press